Frontiers in Heat and Mass Transfer

A COMPARISON OF THE EQUILIBRIUM AND THE DROPLETS BASED NON-EQUILIBRIUM COMPRESSIBLE PHASE CHANGE SOLVERS FOR CONDENSATION OF CARBON DIOXIDE INSIDE NOZZLES

Kapil Dev Choudhary, Shyam Sunder Yadav[†], Mani Sankar Dasgupta

Birla Institute of Technology and Science, Pilani, Rajasthan, 333031, India

ABSTRACT

In the current work, we simulate the condensation of supercritical CO_2 during its high speed flow inside two different converging-diverging nozzles. We use the homogeneous equilibrium method and the classical nucleation theory based non-equilibrium phase change model for this purpose. The simulation results indicate significant influence of the nozzle inlet condition, nozzle shape and the fluid thermophysical behaviour on the non-equilibrium conditions prevailing inside the nozzles. We observe very low, $\sim$0.15 K, supercooling for the flow of CO_2 inside the Claudio Lettieri nozzle compared to the supercooling of $\sim$3 K observed for the Berana nozzle. Very high nucleation rate ($\sim 10^{35}$ nucleation per m^3 per second) is observed before the throat of the nozzles which remains confined to a very small axial distance. The nucleation rate takes much smaller values ($\sim 10^7$ nucleation per m^3 per second) in rest of the nozzle. A maximum of 70 nano meter sized droplets with number densities of the order of 10^{21} droplets per m^3 are predicted inside the nozzles. Liquid mass fraction values between 0.2 to 0.4 are predicted by the solvers inside the nozzles. These results will be useful to the engineering community involved in the design and fabrication of CO_2 based systems.

Keywords: *Compressible phase change; Homogeneous equilibrium model; Droplets based non-equilibrium model; Classical nucleation theory; Transcritical Carbon dioxide; Ansys CFX.*

1. INTRODUCTION

There is recent surge in the use of CO_2 for various industrial applications where it undergoes condensation during certain phases of the working cycle. Examples include the flow of CO_2 inside compressors and turbines used in supercritical Brayton cycle (e.g., Lettieri *et al.* (2018); Lettieri *et al.* (2015); Ameli *et al.* (2018)) and the fracture induced depressurisation of pipelines used for carbon capture, transportation and storage (e.g., Brown *et al.* (2014); Nouri-Borujerdi and Ghazani (2017); Wen *et al.* (2019)). This phase change process is involved in other industrial applications as well which deal with high speed flow of vapors. The flow of steam through nozzles and turbine sections (e.g., Hill (1966); Moses and Stein (1978); Starzmann *et al.* (2018); Grübel *et al.* (2018); Xiao *et al.* (2017)) and the flow of refrigerants inside ejectors for pressure recovery (e.g., Palacz *et al.* (2015); Mazzelli *et al.* (2018); Giacomelli *et al.* (2019)) undergo similar phase transition. A common feature of such high speed flows with phase change is the existence of thermodynamic non-equilibrium conditions. The working fluids attain metastable thermodynamic states and suddenly undergo phase transition causing a condensation shock. The phase change process may be essential for the operation of the devices like condensing ejectors while having undesirable effects on the performance of steam turbines and supercritical CO_2 compressors. The presence of shock waves, shear layers, boundary layer

separation, flow turbulence along with the phase change process make such flows difficult to analyse. There is a need to quantify the condensation behaviour with respect to the distribution of physical quantities like vapor supercooling, droplet nucleation rate, droplet diameter and number density, liquid mass fraction etc. Converging-diverging nozzles are simple devices with no moving parts and ideally suited for performing experimental or simulation based investigations of the phase change process. These are also used in most of the practical applications discussed before. Therefore, to quantify the phase change process of CO_2, we simulate its flow inside converging–diverging nozzles. We use two different solvers available in Ansys CFX for this purpose, namely, the homogeneous equilibrium model based solver and the classical nucleation theory based non-equilibrium phase change solver. In the following, we briefly review the previous works related to the simulation of compressible phase change process focusing mainly on the works based on the homogeneous equilibrium and the non-equilibrium models.

The flow of CO_2 through nozzles and radial compressors has gained attention recently due to its application in the supercritical Brayton cycle and in the carbon capture and storage based technique for atmospheric CO_2 reduction. Such flows involve significant compressibility related effects and undergo phase change around leading edge of the the com-

---
[†]*Corresponding author. Email: ss.yadav@pilani.bits-pilani.ac.in*

pressor blades. Here we summarize some of the most recent numerical works in this area. Ameli *et al.* (2017b) investigated the accuracy of various equations of state and the resolution of real gas property tables for flow inside supercritical radial compressors and turbines. For near critical inlet states, they observed that the Span and Wagner equation gives the most accurate results among the different equations used. Ameli *et al.* (2017a) compared the simulation based results on flow of supercritical CO_2 through a converging–diverging nozzle, the experiments on which were provided by Berana *et al.* (2009). The thermophysical properties of CO_2 in the metastable state were obtained using a bilinear extrapolation of the saturation state data. They observed that the flow becomes supersonic in the converging part of the nozzle just before the throat. They also highlighted the need to constrain the critical radius of the nucleating droplets to around a nano meter. Lettieri *et al.* (2018) experimentally investigated the metastable behaviour of CO_2 during its high speed expansion inside a Laval nozzle. They obtained the Wilson line with the help of optical visualization and laser interferometry based techniques. It was observed that the computational data obtained with the extrapolated Span and Wagner equation of state agree within 2% of the experimentally observed values. Ameli *et al.* (2018) compared the numerical results on the flow of CO_2 through a centrifugal compressor for different resolutions of the real gas property (RGP) table. They compared the CFD based distribution of entropy and density values over the compressor impeller with those obtained from NIST REFPROP (Lemmon *et al.* (2018)). They concluded that the errors in the simulated results decrease as the resolution of the RGP table increases but with increasing instability of the numerical solution procedure.

A significant amount of simulation based work has been performed on CO_2 ejectors which are used for work recovery in supermarket refrigeration systems. Here we briefly discuss the important previous works related to ejector flow simulation. Smolka *et al.* (2013) expressed the heat conduction term in the energy equation in terms of enthalpy. This, combined with the pressure, was used to track the two phases under the homogeneous equilibrium approach. They observed a discrepancy of around 20% in the computed mass flow rates through the motive and the suction nozzles. Banasiak *et al.* (2014) analysed the entropy generation inside a two phase CO_2 ejector based on the homogeneous equilibrium model. They concluded that the oblique shock train and flow turbulence contributed most towards the entropy generation inside the ejector's mixer and diffuser sections. Palacz *et al.* (2015) investigated the accuracy of homogeneous equilibrium method (HEM) for two phase flow through an ejector geometry. They concluded that the HEM model gives accurate results for operating conditions near and above the fluid critical point. The accuracy of the results decreased as the the inlet state was moved near to the saturation line. Palacz *et al.* (2017) compared the simulation data from the homogeneous equilibrium and homogeneous relaxation based phase change approaches with the experimental data on flow through an ejector. It was observed that both the phase change models predicted inaccurate mass flow rates for operating conditions far from the critical point. The HEM approach was found to be more accurate for operating conditions above the critical point. Using the homogeneous relaxation method, Haida *et al.* (2018) investigated the effect of relaxation time parameters on the distribution of pressure, velocity and vapor quality inside an ejector. An increase in the value of the coefficient θ_0 decreased the vapor quality and the pressure inside the diverging portion of the motive nozzle. It also strongly influenced the shock formation and the flow process inside the mixing zone.

Recent simulation based works have considered the high speed condensation of vapor of one fluid inside another carrier gas. Using Ansys Fluent, Xiao *et al.* (2017) simulated the condensation of water vapor present in wet natural gas inside a nozzle. A maximum nucleation rate of 10^{23} droplets per m^3 per second and droplet number density of 10^{19} droplets per m^3 are observed inside the nozzle. Zheng *et al.* (2018) numerically investigated the condensation of CO_2 during the high speed

flow natural gas in a supersonic separator. A maximum nucleation rate of 10^{21} droplets per m^3 per second and droplet diameter of 10^{-7} m are observed inside the separator. Du and Hu (2020) investigated the effect of non-condensable gases on the phase change process of CO_2 inside an evaporator. They theoretically showed that non-condensable gases convert the nucleation mechanism from homogeneous to heterogeneous and promote the phase change process.

From this brief literature survey, we observe that most of the simulation based works on condensation of CO_2 have used the homogeneous equilibrium and the homogeneous relaxation based approaches. These approaches do not give an idea about the distribution of the nucleation rate, the number density and the diameter of the droplets. Although the classical nucleation theory has been widely applied for the condensation of steam, its use for the phase change of CO_2 is more recent. In the current work, we simulate the phase change process of CO_2 inside two different converging-diverging nozzles. We use two different compressible phase change solvers from the commercial flow solver Ansys CFX for this purpose. These are the homogeneous equilibrium based solver and the classical nucleation theory based non-equilibrium phase change solver. Based on the simulations, we predict the distribution of following physical quantities inside the nozzles: the supercooling levels attained by CO_2; the nucleation rate; the droplet diameter and number density; and finally, the liquid mass fraction. This work is organized as follows: in Section 2, we describe the computational domains and the boundary conditions; in Section 3, we present the equations which govern the phase change of CO_2 under the homogeneous equilibrium and the classical nucleation theory based non-equilibrium solvers; in Section 4, we present the details on the solver settings in Ansys CFX and the CO_2 thermophysical properties; in Section 5, we discuss the results obtained by us using the simulation setup; and finally in Section 6, we conclude this work.
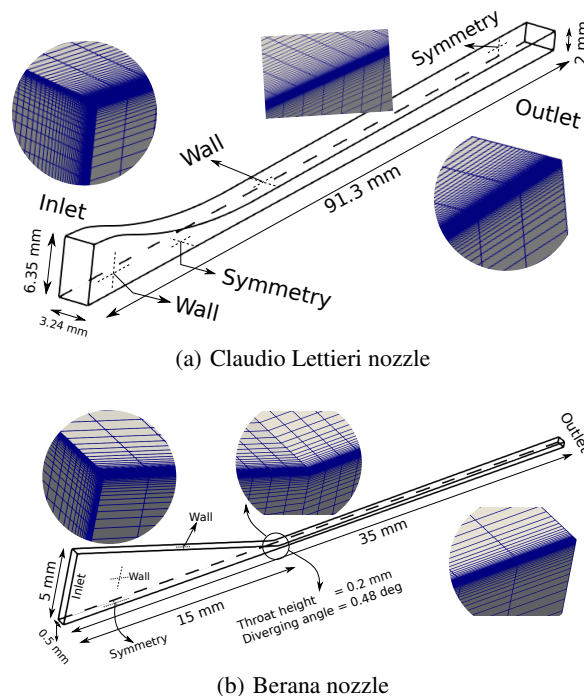

(a) Claudio Lettieri nozzle

(b) Berana nozzle

Fig. 1 The computational domains for the flow of CO_2 inside converging–diverging nozzles: (a) Lettieri *et al.* (2018) nozzle and (b) Berana *et al.* (2009) nozzle. Two symmetry planes are used inside each nozzle in order to reduce the computational effort.

Table 1 Boundary and initial conditions for the two nozzle cases.

Variable	Claudio Lettieri	Berana
Inlet pressure	80 bar	90 bar
Outlet pressure	28 bar	35.5 bar
I.C. pressure	55 bar	65 bar
Inlet temperature	311 K	318 K
I.C. temperature	311 K	318 K

2. COMPUTATIONAL DOMAINS AND BOUNDARY CONDITIONS

In this section, we discuss the computational domains and the mesh related details for the two different converging–diverging nozzles used by us. The very first case considers the flow of CO_2 inside a converging-diverging nozzle used by Lettieri *et al.* (2018), the computational domain for which is shown in Fig. 1(a). A structured, body fitted, curvilinear mesh is generated inside the domain with smaller height of mesh elements near the walls. A total of 284739 hexahedral cells are generated in the domain using GMSH which is an open source mesh generator developed by Geuzaine and Remacle (2009). The wall mesh thickness is gradually varied normal to the walls, the non-dimensional wall distance y^+ varies from 8 near the throat region to 4 in the diverging potion under fully developed flow conditions. The domain shown in Fig. 1(b) investigates the flow of CO_2 through a converging-diverging nozzle having straight walls and experimentally studied by Nakagawa *et al.* (2008), Berana *et al.* (2009). The mesh for this case has a total of 360477 hexahedral cells. The non-dimensional wall distance y^+ in this case varies from a maximum of 14 near the throat region to a minimum of 2 in the diverging portion of the nozzle under fully developed flow situation. In order to reduce the computational effort, we simulate the flow inside one fourth of the actual physical domains by using symmetry boundary conditions as shown in the figures. The various initial and boundary conditions at the inlet and outlet of the domains are shown in Table (1).

3. GOVERNING EQUATIONS

In this section, we describe the equations which govern the phase change process of a vapor under the homogeneous equilibrium and the classical nucleation theory based non-equilibrium models. The following discussion is based on Gerber (2008) and the Ansys CFX theory guide (ANSYS (2017)).

3.1. Equilibrium phase change solver

The homogeneous model assumes that the inter-phase transport processes occur at a much faster time scale compared to the fluid flow time scale so that there exists a mechanical, thermal and chemical potential equilibrium between the phases. The consequences of this assumption are the equality of the velocity, pressure, temperature and the Gibbs free enthalpy of the phases in the grid cells containing both the phases. The two phases are treated as a single fluid mixture with different thermophysical properties depending on the spatial distribution of the individual phases. Because of the mechanical and the thermal equilibrium between the phases, the homogeneous equilibrium model does not require an explicit formulation of the interfacial transport processes. In the following, the subscript l stands for the liquid phase, v stand for the vapor phase and m stands for their mixture.

The mass conservation equation for the two-phase mixture is given by

$$\frac{\partial \rho_m}{\partial t} + \nabla \cdot \rho_m \vec{U} = 0, \tag{1}$$

where $\rho_m = \alpha_l \rho_l + \alpha_g \rho_g$ is the mixture density and α is the volume fraction of the phases with the constraint $\alpha_l + \alpha_g = 1$. The momentum

conservation equation for the two phase mixture is given by

$$\frac{\partial \rho_m \vec{U}}{\partial t} + \nabla \cdot \rho_m \vec{U}\vec{U} = \nabla \cdot \left\{ \mu_m (\nabla \vec{U} + \nabla \vec{U}^T) - \frac{2}{3} \mu_m \nabla \cdot \vec{U} \mathbf{I} \right\}$$
$$- \nabla p + S, \tag{2}$$

where $\mu_m = \alpha_l \mu_l + \alpha_v \mu_v$ is the viscosity of the mixture and S holds any other relevant momentum source term like that due to gravity. Ansys CFX solves for two different 'total enthalpy' based equations instead of solving a single mixture enthalpy equation. The equations for the total enthalpy of the liquid and the vapor phase are respectively given by

$$\frac{\partial \alpha_l \rho_l h_{t,l}}{\partial t} - \alpha_l \frac{\partial p}{\partial t} + \nabla \cdot \alpha_l \rho_l \vec{U} h_{t,l} = \nabla \cdot \alpha_l k_l \nabla T + \alpha_l \nabla \cdot \tau_l \cdot \vec{U}$$
$$+ Q_l, \tag{3}$$

$$\frac{\partial \alpha_g \rho_g h_{t,g}}{\partial t} - \alpha_g \frac{\partial p}{\partial t} + \nabla \cdot \alpha_g \rho_g \vec{U} h_{t,g} = \nabla \cdot \alpha_g k_g \nabla T + \alpha_g \nabla \cdot \tau_g \cdot \vec{U}$$
$$+ Q_g. \tag{4}$$

In the above equations, Q_l and Q_g denote the heat transfer to the respective phases across the interface. The mass fraction of the vapor is calculated based on the enthalpy of the mixture using the following equation:

$$x = \frac{h_m - h_{sat,l}(p)}{h_{sat,v}(p) - h_{sat,l}(p)}. \tag{5}$$

This implies that a grid cell contains sub-cooled liquid if $x < 0$, super-heated vapor if $x > 1$ and the two phase mixture if $0 \le x \le 1$. The different thermophysical properties of the fluid are calculated based on the vapor mass fraction value.

3.2. Droplets based non-equilibrium phase change solver

The droplets based non-equilibrium phase change solver computes for the homogeneous nucleation and growth of droplets in a rapidly expanding fluid vapor. This model calculates the droplet diameter and the droplet number density as part of the solution. The mathematical formulation of the model involves equations for the continuous and the dispersed phase which are assumed to move at the same speed. In the following, the subscript c stands for continuous phase which is the vapor phase in our case while the subscript d stands for dispersed phase which is the condensed liquid phase in the form of droplets. The mass conservation equation for the continuous phase is given by

$$\frac{\partial \alpha_c \rho_c}{\partial t} + \nabla \cdot \alpha_c \rho_c \vec{U} = -S_m - \alpha_c \hat{m}_d \mathbf{J}_d, \tag{6}$$

while that for the dispersed phase is given by

$$\frac{\partial \alpha_d \rho_d}{\partial t} + \nabla \cdot \alpha_d \rho_d \vec{U} = S_m + \alpha_d \hat{m}_d \mathbf{J}_d. \tag{7}$$

In the above equations, S_m represents the interfacial mass transfer term, $\mathbf{J}_d$ is the critical nucleation rate and $\hat{m}_d$ is the nucleated droplet mass based on the critical radius $\hat{R}_d$. The constraint $\alpha_c + \alpha_d = 1$ applies for the volume fractions of the two phases. The analysis by Bakhtar *et al.* (2005) provides the following expression for the critical nucleation rate:

$$\mathbf{J}_d = q_c \frac{\rho_c^2}{\rho_d} \left(\frac{2\sigma(T_c)}{\pi m_m^3} \right)^{1/2} \times e^{-\hat{G}b}. \tag{8}$$

Here q_c is an empirical constant which is taken equal to one in this work, m_m is the mass of a single molecule of CO_2, $\hat{G}b$ is the Gibbs number at the critical drop radius and is given by

$$\hat{G}b = \frac{\Delta \hat{G}}{k_B T_c}. \tag{9}$$

In this equation, k_B is the Boltzmann constant, $\Delta \hat{G}$ is the change in the Gibbs free enthalpy of the supercooled vapor during the formation of a droplet of critical radius, $\hat{R}_d$, which are respectively given by

$$\Delta \hat{G} = \frac{4}{3} \pi \hat{R}_d^2 \sigma(T_c), \quad (10)$$

and

$$\hat{R}_d = \frac{2\sigma(T_c)}{\rho_d \bar{R} T_c \ln\left(\frac{P_c}{P_{\text{sat}}(T_c)}\right)}. \quad (11)$$

In the above equations, $\bar{R}$ is the gas constant for CO_2 vapor, $P_{\text{sat}}(T_c)$ is the saturation pressure at the vapor temperature, $\sigma(T_c)$ is the surface tension coefficient which is a function of the continuous phase temperature, the expression for which is given later. Therefore, we get the expression for the Gibbs number at critical drop radius as

$$\hat{G}b = \frac{16\pi\sigma^3(T_c)}{3 k_b T_c^3 \left[\rho_d \bar{R} \ln\left(\frac{P_c}{P_s(T_c)}\right)\right]^2}. \quad (12)$$

Further details on the theory and application in the context of steam condensation can be found in Bakhtar *et al.* (2005), Starzmann *et al.* (2018) and Grübel *et al.* (2018).
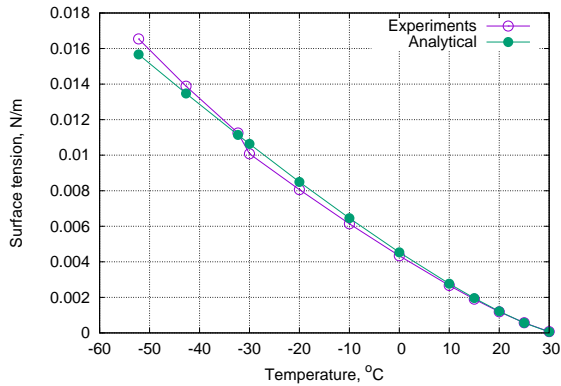

Fig. 2 Variation of surface tension coefficient of Carbon dioxide with temperature while the analytical expression is taken from Miqueu *et al.* (2000). The experimental data is based on Jianxin and Yigang (2009).

The surface tension coefficient σ between the liquid and the vapor states of CO_2 is a function of temperature and is implemented in the current work based on the following equation from Miqueu *et al.* (2000)

$$\sigma(T) = k_B T_{cr} \left(\frac{N_A}{V_{cr}}\right)^{2/3} \times (4.35 + 4.14\omega) T_r^{1.26}$$
$$\times \left(1 + 0.19 T_r^{0.5} - 0.25 T_r\right). \quad (13)$$

In this equation, N_A is the Avogadro number, $V_{cr} = 0.00214$ m^3/kg is the critical volume, $\omega = 0.239$ is the acentric factor, $T_r = 1 - \frac{T}{T_{cr}}$ with $T_{cr} = 304.13$ K being the critical temperature of CO_2. The variation of the surface tension coefficient with temperature based on Eq. (13) and the actual experimental data are shown in Fig. (2). Equation (13) is implemented as a CEL expression in Ansys CFX based on its reference guide, Ansys (2017).

The momentum conservation equation is similar to that for the homogeneous equilibrium model and is given by

$$\frac{\partial \rho_m \vec{U}}{\partial t} + \nabla \cdot \rho_m \vec{U}\vec{U} = \nabla \cdot \left\{ \mu_m (\nabla \vec{U} + \nabla \vec{U}^T) - \frac{2}{3} \mu_m \nabla \cdot \vec{U} \mathbf{I} \right\}$$
$$- \nabla p + S_p, \quad (14)$$

The continuous phase energy equation is given by

$$\frac{\partial \alpha_c \rho_c h_{t,c}}{\partial t} - \alpha_c \frac{\partial p}{\partial t} + \nabla \cdot \alpha_c \rho_c \vec{U} h_{t,c} = \nabla \cdot (\alpha_c k_c \nabla T) + S_h, \quad (15)$$

while that for the dispersed phase is given by

$$\frac{\partial \alpha_d \rho_d h_{t,d}}{\partial t} - \alpha_d \frac{\partial p}{\partial t} + \nabla \cdot \alpha_d \rho_d \vec{U} h_{t,d} = \nabla \cdot (\alpha_d k_d \nabla T) - S_h. \quad (16)$$

The equation governing the number density of the droplets is given by

$$\frac{\partial \rho_d N_d}{\partial t} + \nabla \cdot \rho_d \vec{U} N_d = \alpha_c \rho_d \mathbf{J}_d, \quad (17)$$

where the droplets move at the mixture velocity because of the no slip condition assumed between the phases. The droplet radius growth rate is given by

$$\frac{dR_d}{dt} = \frac{k_c}{R_d \rho_d (1 + \xi \, \text{Kn})} \left(\frac{T_d - T_c}{h_c - h_d}\right), \quad (18)$$

where ξ is an empirical constant and Kn is the Knudsen number which is included to take into account the droplet size variation from the molecular to the continuum scales. For very small droplets ($d \leq 1\mu$m), the dispersed phase energy equation, Eq. (16), is discarded in favour of the droplet temperature, T_d, which is calculated using

$$T_d = T_{\text{sat}}(p) - T_{\text{sc}} \frac{R_d^*}{R_d}. \quad (19)$$

In this equation, $T_{\text{sat}}(p)$ is the saturation temperature as a function of pressure p, T_{sc} is the supercooling level in vapor phase, R_d is the droplet radius, and finally, R_d^* is the critical droplet radius. The term in Eqs. (6) and (7), related to the droplet growth due to mass transfer across the interface, is given by

$$S_m = \rho_d \beta_d \frac{dR_d}{dt} \quad (20)$$

where $\beta_d = \frac{3\alpha_d}{R_d}$ is the interfacial area available per unit volume. The source term in the equations for the total enthalpy of the phases, Eqs. (15), (16), is given by

$$S_h = -S_m h_{t,u} + \beta_d q_d'' \quad (21)$$

where $h_{t,u}$ is the upwinded total enthalpy whose value depends on the direction of mass transfer across the interface. The very small droplets ($R_d \leq 1\mu$) are assumed to have a uniform temperature with all the heat transfer q_d'' occurring in the continuous phase during evaporation and condensation with the heat flux calculated based on

$$q_d'' = \frac{k_c}{R_d(1 + \xi \, Kn)} (T_d - T_c). \quad (22)$$

In the following section, we describe the solver settings used for the two compressible phase change solvers in Ansys CFX.

4. SOLVER SETTINGS AND THERMOPHYSICAL PROPERTIES

In this section, we briefly describe the various options used for the spatial and temporal discretization in Ansys CFX. The spatial discretization in Ansys CFX is based on control volume based finite element method under which the flow variables are stored at mesh nodes. The variation of the flow variables along the cell faces is given by geometric or parametric shape functions. The pressure and velocity are interpolated using a trilinear scheme while the pressure-velocity coupling is enforced using high resolution Rhie-Chow type scheme. The convective part of the mass, momentum and energy equations is discretized using high resolution scheme. The first order accurate implicit Euler method is used for temporal discretization. The volume fraction equation is solved in a coupled manner with the mass, momentum and energy equations with a residual and conservation target of 10^{-4}. The vapor phase heat transfer is based on the total energy formulation. The surface tension coefficient is

Table 2 RGP table bounds for CO_2 thermophysical data.

Variable	Value
Min. Temperature	220.0 K
Max. Temperature	800.0 K
Min. Pressure	6.0 bar
Max. Pressure	160.0 bar
No. of points	500

calculated based on the vapor temperature. The particles based homogeneous nucleation model is used for the phase change process. The liquid phase heat transfer is calculated based on the small droplets assumption.

The non-equilibrium solver requires fluid thermophysical properties in the subcooled state. This necessitates the use of a property database or an equation of state for the vapor phase amenable to extrapolation in the subcooled region. As per the Ansys solver theory guide (ANSYS (2017)), the IAPWS database for water and the Redlich-Kwong family of equation of state for CO_2 are capable of such extrapolations but the latter's accuracy is unreliable near the critical point and for subcooled liquid states. For the equilibrium solver, we used the real gas properties of CO_2 based on NIST REFPROP (Lemmon *et al.* (2018)). The temperature and pressure bounds for the RGP table are given in Table (2). The Soave-Redlick-Kwong equation of state, Soave (1972), is used for the thermophysical data required for non-equilibrium calculations, the table bounds for which are shown in Table (2). One has to use the expert parameter `realeos liquid prop = 2` in Ansys CFX to force the solver to read the subcooled liquid properties based on the cubic equation of state. The parameters given in the Table (2) give a resolution of $\Delta T = 1.16$ K for temperature and $\Delta p = 0.31$ bar for CO_2. Similar resolutions were used by Ameli *et al.* (2018) for the simulation of flow inside supercritical CO_2 turbines. Since the actual flow inside the nozzles is turbulent, we used the $k - \Omega$ SST model with defaults model parameters for calculating the various turbulent fluxes. This model has performed satisfactorily for various internal and external, high Reynolds number flows (e.g., Bartosiewicz *et al.* (2005); Mazzelli *et al.* (2015); Croquer *et al.* (2016a,b); Pang *et al.* (2016)). A 5% turbulence intensity is assumed at the inlet of the domain.

For the non-equilibrium solver, a converged solution is obtained easily by adopting the following approach. First, the nucleation process is switched-off in the solver, allowing time steps of $\sim 10^{-5}$ second to be used for attaining vapor supercooling in the domain. Afterwards, the nucleation is switched-on allowing phase change to be simulated at time steps of the order of 10^{-9} second. Lastly, as mentioned in Ameli *et al.* (2017a), the critical radius of the droplets is calculated in Ansys CFX based on the Gibbs free enthalpy change of the continuous phase ($\Delta G_c = g(P_c, T_c) - g(P_{\text{sat}}, T_c)$) using

$$R_d^* = \frac{2\sigma}{\rho_d \Delta G_c}. \tag{23}$$

Near the critical point, the Gibbs free energy change becomes very small due to which the critical radius value become as high as 10^{-3} m. In order to avoid such nonphysical values, an 'expert parameter' is used in the solver in order to constrain the critical radius to a maximum of 10^{-8} m. In the following section, we present the various results obtained by us based on the simulations performed with Ansys CFX.

5. RESULTS AND DISCUSSIONS

In this section, we discuss the various results obtained with Ansys CFX on the phase change process of CO_2 inside the two converging–diverging nozzles. First we present the results on the flow of supercritical CO_2 through a nozzle, the experiments on which were performed by Lettieri *et al.* (2018). We call this case as the Lettieri test case. Next we present

the simulation results related to the flow of supercritical CO_2 in a converging diverging nozzle with straight walls, the experiments on which were performed by Berana *et al.* (2009). We call this particular case as the Berana test case. Based on the different geometrical shapes, expansion rates of the working fluids and the inlet conditions, different amount of supercooling levels are expected inside the nozzles.
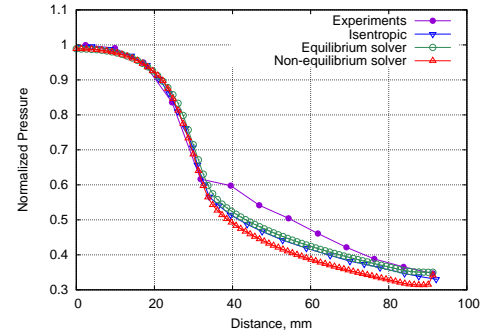
5.1. Lettieri nozzle case

Fig. 3 Variation of pressure along the Claudio Lettieri nozzle center line based on the experiments conducted by Lettieri *et al.* (2018) and the two compressible phase change solvers in Ansys CFX. The pressure at the nozzle inlet (8 MPa) is used for normalization.

Figure (3) shows the experimental pressure distribution along the center line of the Claudio Lettieri nozzle along with those based on the numerical simulations using the equilibrium and non-equilibrium phase change solvers in Ansys CFX. As can be seen, the equilibrium solver gives a better pressure distribution in the nozzle which may be due to the more accurate fluid thermophysical data coming from NIST REFPROP (Lemmon *et al.* (2018)). The non-equilibrium solver under-predicts the pressure in the diverging part of the nozzle which can be attributed mostly to the use of cubic equation of state for the thermophysical properties of CO_2. Other parameters of the solver like the maximum critical radius, bulk nucleation tension factor, interphase transfer model may also be playing a role here. Figure (4) shows the distribution of the pressure
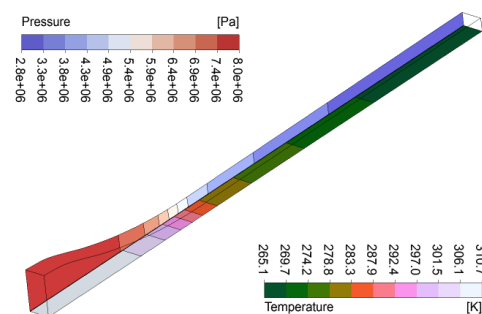

Fig. 4 Distribution of the absolute pressure and the vapor temperature inside the Claudio Lettieri nozzle calculated based on the non-equilibrium solver.

and vapor temperature contours on the symmetry planes of the Lettieri nozzle based on the non-equilibrium solver. The fluid cools down as it expands inside the nozzle with a minimum temperature equal to 265 K at the exit of the nozzle. A similar distribution is obtained with the equilibrium solver as well. Figure (5) shows the distribution of the Mach number and the local speed of sound for the vapor phase of CO_2 in the Claudio Lettieri nozzle. It can be seen that flow becomes supersonic only in the diverging portion of the nozzle while it is subsonic near the throat of the nozzle. This is in spite of the fact that the local speed of sound is lowest in
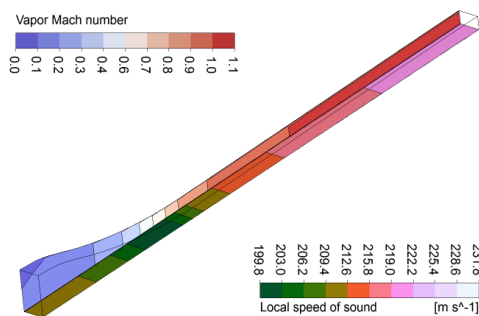
Fig. 5 Distribution of the vapor Mach number and local speed of sound inside the Claudio Lettieri nozzle calculated based on the non-equilibrium solver.

the throat region implying the flow velocity must also be small in that region. Figure (6) compares the liquid mass fraction distribution inside the
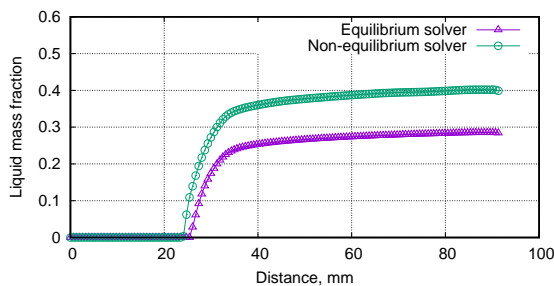

Fig. 6 Comparison of the liquid mass fraction distribution along the Lettieri nozzle center line based on the equilibrium and the non-equilibrium solvers.

Lettieri nozzle based on the equilibrium and the non-equilibrium solvers. It can be seen that the maximum liquid mass fraction at the nozzle outlet is around 0.3 based on the equilibrium solver while it is equal to 0.4 with the non-equilibrium solver.
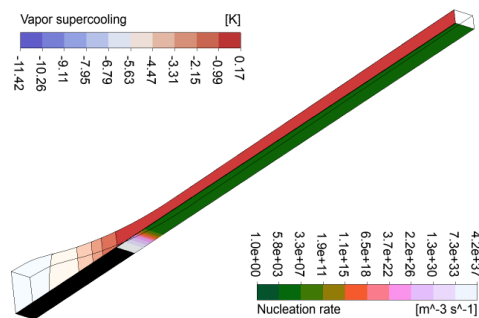

Fig. 7 Contours of the vapor supercooling and the nucleation rate inside the Lettieri nozzle based on the non-equilibrium solver. The nucleation rate is zero in the converging portion of the nozzle and becomes very high when the vapor becomes supercooled.

The non-equilibrium solver gives information on several other parameters which are discussed in the following. Figure (7) shows the distribution of the vapor supercooling and the nucleation rate on two mutually perpendicular, symmetry planes of the Lettieri nozzle. It can be noted that there exist very small (~ 0.15 K) vapor supercooling inside the nozzle after the phase change process. This is due to the near critical condition (80 bar, 311 K) of CO_2 at the inlet to the nozzle where the spinodal limit itself is near to the saturated vapor line. This probably

hints at the low overall non-equilibrium conditions existing in the nozzle. The figure also shows that there is a very high droplet nucleation intensity ($\sim 10^{35}$ nucleation per m^3 per second) confined to a narrow portion of the nozzle length before the throat which falls steeply to a much smaller, almost constant value ($\sim 10^7$ nucleation per m^3 per second) in the diverging part of the nozzle. The line plot shown in Fig. (8) represent the same information along the Lettieri nozzle center line. It can be observed in the figure that the degree of liquid subcooling is also very small ~ 0.15 K. Figures (9) and (10) show the distribution of the droplet diameter and
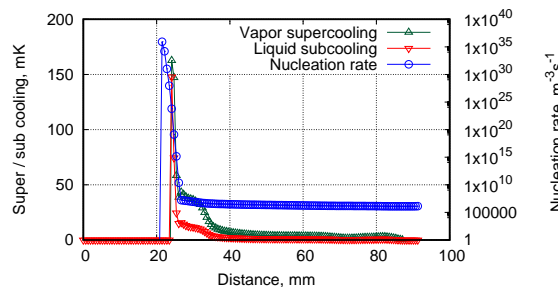

Fig. 8 Distribution of the liquid subcooling, vapor supercooling and the nucleation rate along the Lettieri nozzle center line based on the non-equilibrium solver.
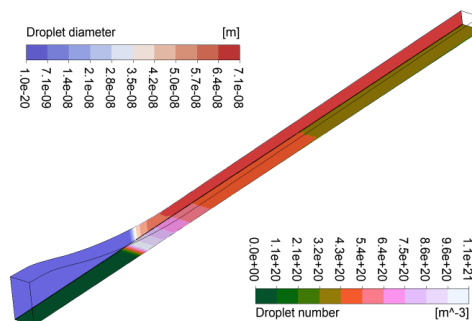

Fig. 9 Contours of the droplet diameter and droplet number density inside the Claudio Lettieri nozzle calculated based on the non-equilibrium solver.
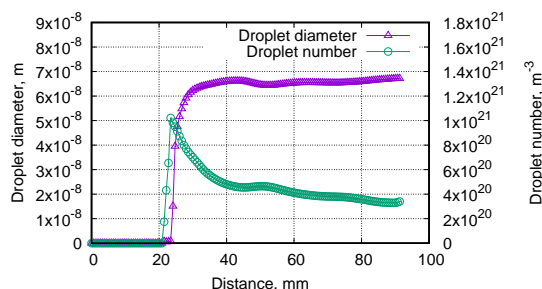

Fig. 10 Distribution of the droplet diameter and droplet number density along the Claudio Lettieri nozzle center line calculated based on the non-equilibrium solver.

the droplet number density inside the Lettieri nozzle. It can be seen that the droplet size is the smallest near the nucleation zone which then increases steeply to around 65 nano meter in a very short axial distance. Similarly, starting from a negligible value at around 20 mm, the number density of the droplets increases steeply in a very small axial distance, and afterwards, decreases gradually along the nozzle length.
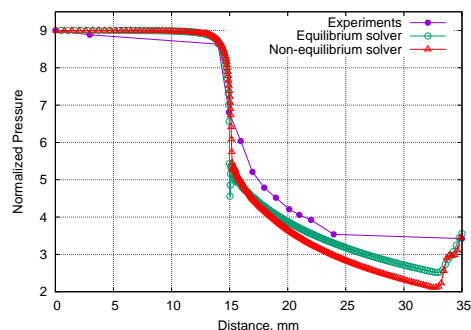
5.2. Berana nozzle case

Fig. 11 Variation of pressure along the Berana nozzle center line from the experiments by Berana *et al.* (2009) and the current simulations. A pressure of 1 MPa is used for normalization.

Here we briefly discuss the results on the phase change process of CO_2 inside the Berana nozzle, the experiments on which were performed by Berana *et al.* (2009). Figure (11) compares the simulation based pressure distribution in the Berana nozzle with the experimentally obtained values. It can be noticed that the equilibrium solver again predicts a better pressure distribution compared to that obtained with the non-equilibrium solver in spite of the better theoretical formulation of the latter. This can be attributed to two reasons. First, the equilibrium solver uses the REFPROP (Lemmon *et al.* (2018)) based more accurate thermophysical properties of CO_2 in the form of RGP tables. Second, the non-equilibrium solver involves various empirical parameters in the theoretical formulation whose values are unknown before-hand. As can be seen in Fig. (11), the equilibrium solver predicts a shock wave located immediately downstream to the throat as revealed by the kink in the pressure distribution curve. Both the equilibrium and the non-equilibrium solvers under-predict the pressure values after the throat of the nozzle. It may be also be noted here that no experimental data is available for pressure distribution near the exit of the nozzle. Figure (12) shows the corresponding pressure contours along with the distribution of vapor temperature on the two symmetry planes inside the Berana nozzle. It should be noted that the vapor temperature increases as the throat is approached starting from a value of 318.15 K at the inlet boundary. After the throat, the temperature decreases along the diverging portion of the nozzle.
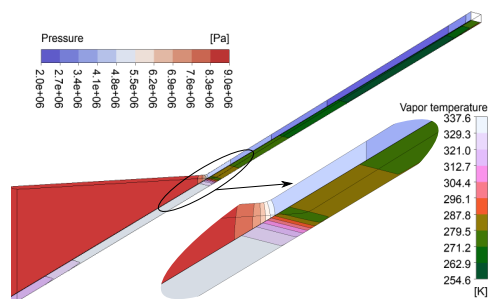

Fig. 12 Distribution of pressure and vapor temperature inside the Nakagawa nozzle based on the non-equilibrium solver. The inlet temperature is equal to 318.15 K. The temperature first increases in the converging part of the nozzle and then decreases after the throat.

Based on the non-equilibrium solver, Ameli *et al.* (2017a) simulated flow inside a two dimensional geometry of the Berana nozzle and observed that the flow becomes supersonic inside the converging portion of the nozzle, that is, before the throat of the nozzle. This is not the case
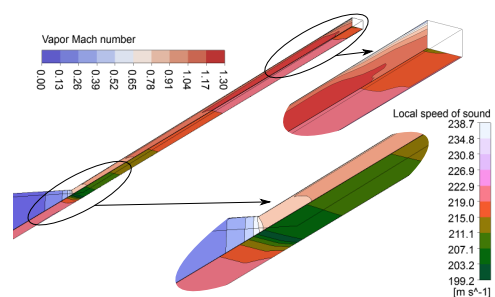

Fig. 13 Contours of the local speed of sound and the Mach number inside the Nakagawa nozzle based on the non-equilibrium solver.

when a three dimensional computational domain is used as can be seen in Fig. (13) which shows a Mach number of around 0.65 at the throat. Information on the distribution of the liquid mass fraction of CO_2 along the Berana nozzle center line can be gained from Fig. (14). The figure shows that the equilibrium solver predicts a higher value (~ 0.2) of maximum liquid mass fraction distribution inside the nozzle compared to the non-equilibrium solver which gives a maximum value of around 0.16. Also, the liquid fraction starts increasing abruptly from a value of 0.1 under the equilibrium solver while it increases gradually from zero under the non-equilibrium solver. The liquid mass fraction decreases because of the viscous heating by the shock wave whose presence can be guessed from the pressure variation in Fig. (11).
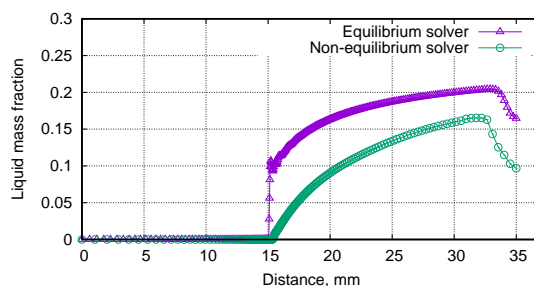

Fig. 14 Comparison of the liquid mass fraction distribution along the Berana nozzle center line based on the equilibrium and the non-equilibrium solvers. The phase change process starts exactly at the throat of the nozzle.
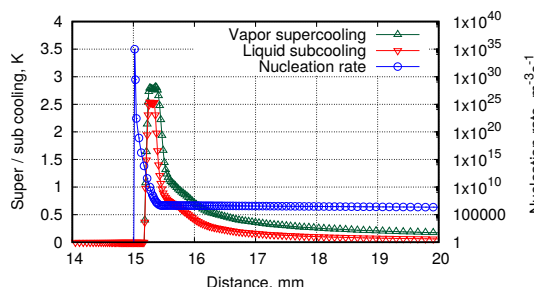
Fig. 15 Distribution of the vapor supercooling and the nucleation rate along the Berana nozzle center line calculated based on the non-equilibrium solver.

Figure (15) shows the variation of supercooling / subcooling levels achieved by the phases of CO_2 and the nucleation rate of the droplets along the center line of the Berana nozzle. In contrast to the Lettieri nozzle case, the supercooling level here is around 3 K which shows that non-equilibrium effects are stronger in this case. This may be due to

the higher pressure and temperature values (90 bar, 318 K) at the inlet to the nozzle so that the state is farther from the critical point compared to that in the Lettieri case. However, it should be noted that the vapor supercooling and the liquid subcooling quickly becomes very small further downstream the nozzle showing that the flow equilibrates in a short distance ($\sim$2 mm) after the throat. The nucleation rate starts with a very high value (10^{35} nucleation per m^3 per second) and then falls steeply like in the Claudio Lettieri case. Afterwards, the nucleation process becomes almost constant further downstream in the nozzle with a value of around 10^6 nucleation per m^3 per second.

Figure (16) shows the variation of drop diameter and their number density along the center line of the Berana nozzle . As can be seen, the droplet number density starts with a high value ($\sim 10^{20}$ droplets per m^3) at the throat followed by a sharp decrease before the kink. Afterwards, the droplet number density decreases gradual along the downstream of the nozzle. The size of the droplets increase gradually to 70 nano meter along the length of the nozzle starting from smaller values at the throat. It may be noted that the droplet diameter decreases while the droplet number density increases near the exit of the nozzle. This may be due to a shock wave existing in the diverging portion of the nozzle just before the outlet as can be seen from the Mach number contours in Fig. (13).
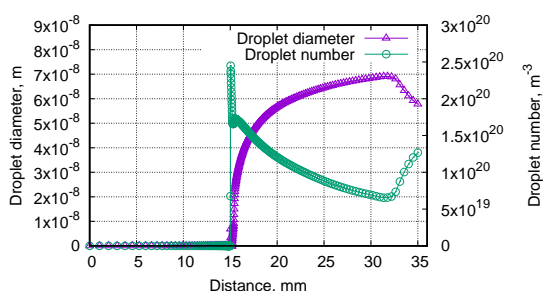

Fig. 16 Distribution of the droplet diameter and the droplet number density along the Berana nozzle center line based on the non-equilibrium solver.

6. CONCLUSIONS

To summarize the current work, we compared two different compressible phase change solvers in Ansys CFX, namely, the equilibrium phase change solver and the classical nucleation theory based non-equilibrium solver for the phase change process of CO_2 inside two different nozzles. The aim of the work was to gain an understanding about the capability and accuracy of the flow solvers for simulating the compressible, high speed flow of CO_2 with phase change inside nozzles. Our experience is summarized as follows. The droplets based non-equilibrium solver needs thermodynamic data from the metastable states for simulating the non-equilibrium conditions inherent in such flows. The solver works well with cubic equations of state but requires fine tuning of several 'expert parameters' for obtaining correct results. The equilibrium solver is more robust and more accurate with respect to prediction of pressure inside the nozzles with REFPROP based real gas property data for CO_2. Compared to experimental data, the solvers under-predicts the pressure distribution inside the nozzles. The simulation results indicate significant influence of the nozzle inlet condition, nozzle shape and fluid thermophysical behaviour on the non-equilibrium effects existing inside the nozzles. For example, we observe very low ($\sim$ 0.15 K) supercooling for the flow of CO_2 inside the Claudio Lettieri nozzle compared to the supercooling ($\sim$ 3 K) observed for the Berana nozzle. The nucleation process inside the nozzles is observed to start abruptly with a very high rate ($\sim 10^{35}$ nucleation per m^3 per second) which remains confined to a very small axial distance and takes much smaller values ($\sim 10^7$ nucleation per m^3 per second) in rest of the nozzle. The non-equilibrium effects are also confined

to a smaller portion of the nozzle and the vapor flow quickly equilibrates itself along the downstream of the nozzle. A maximum of 65 to 70 nano meter sized droplets and number densities of the order of 10^{21} droplets per m^3 are predicted inside the nozzles. Liquid mass fraction values ranging from 0.2 to 0.4 are predicted inside the nozzles.

In general, the solvers are able to simulate compressible, high speed phase change problems with acceptable accuracy which depends on several factors, among which, the use of real gas property database is the most important one. There is a need for a thorough investigation of the effect of different 'expert parameters' which control the behaviour of the non-equilibrium solver. The experience gained here is being used to study the flow of supercritical CO_2 inside an ejector geometry.

NOMENCLATURE

p	pressure (N/m^2)
h	enthalpy (J/kg)
k	thermal conductivity ($W/m \cdot K$)
m_m	mass of a CO_2 molecule (7.308×10^{-26} kg)
Q	interfacial heat transfer (W/m^3)
q''	heat flux (W/m^2)
$\vec{U}$	Velocity (m/s)
R_g	specific gas constant ($J/kg \cdot K$)
$\mathbf{J}$	Nucleation rate (droplet/m^3/s)
t	time (s)
T	temperature (K)
ΔG	Gibbs free energy change (J/kg)
N	number density of droplets (droplet/m^3)
S	momentum source term
S_m	interfacial mass transfer
S_p	interfacial momentum transfer
S_h	interfacial heat transfer
$\hat{m}$	nucleated droplet mass (kg)
x	vapor mass fraction
R	droplet radius (m)
$\bar{R}$	gas constant for CO_2 vapor (0.1889 kJ/kg $\cdot$ K)
N_A	Avogadro number (6.022×10^{23}/mol)
k_B	Boltzmann constant (1.380649×10^{-23} J/K)
Kn	Knudsen number
$\hat{Gb}$	critical Gibbs number

Greek Symbols

ρ	density (kg/m^3)
μ	viscosity ($N \cdot s/m^2$)
τ	viscous stresses (N/m^2)
σ	surface tension coefficient (N/m)
α	volume fraction
β	interfacial area per unit volume (1/m)
ω	acentric factor
ξ	empirical constant
ϕ	supersaturation ratio

Superscripts

$*$	critical value
T	transpose

Subscripts

m	two phase mixture
g	vapor phase
l	liquid phase
c	continuous phase
d	dispersed phase
cr	critical state
t	total
u	upwinded value
sat	saturation state
sc	supercooling
ss	supersaturation

REFERENCES

Ameli, A., Afzalifar, A., and Turunen-Saaresti, T., 2017a, "Non-equilibrium condensation of supercritical carbon dioxide in a converging-diverging nozzle," *Journal of Physics: Conference Series*, vol. 821, 012025, IOP Publishing.
https://doi.org/10.1088/1742-6596/821/1/012025.

Ameli, A., Turunen-Saaresti, T., and Backman, J., 2018, "Numerical investigation of the flow behavior inside a supercritical CO2 centrifugal compressor," *Journal of Engineering for Gas Turbines and Power*, **140**(12), 122604.
https://doi.org/10.1115/1.4040577.

Ameli, A., Uusitalo, A., Turunen-Saaresti, T., and Backman, J., 2017b, "Numerical Sensitivity Analysis for Supercritical CO2 Radial Turbine Performance and Flow Field," *Energy Procedia*, **129**, 1117–1124.
https://doi.org/10.1016/j.egypro.2017.09.233.

ANSYS, 2017, "ANSYS CFX theory guide 18.1," .

Ansys, C., 2017, "Reference Guide, Release 18.1," *ANSYS Inc, Canonsburg, PA*.

Bakhtar, F., Young, J., White, A., and Simpson, D., 2005, "Classical nucleation theory and its application to condensing steam flow calculations," *Proceedings of the Institution of Mechanical Engineers, Part C: Journal of Mechanical Engineering Science*, **219**(12), 1315–1333.
https://doi.org/10.1243/095440605x8379.

Banasiak, K., Palacz, M., Hafner, A., Buliński, Z., Smołka, J., Nowak, A.J., and Fic, A., 2014, "A CFD-based investigation of the energy performance of two-phase R744 ejectors to recover the expansion work in refrigeration systems: An irreversibility analysis," *International Journal of Refrigeration*, **40**, 328–337.
https://doi.org/10.1016/j.ijrefrig.2013.12.002.

Bartosiewicz, Y., Aidoun, Z., Desevaux, P., and Mercadier, Y., 2005, "Numerical and experimental investigations on supersonic ejectors," *International Journal of Heat and Fluid Flow*, **26**(1), 56–70.
https://doi.org/10.1016/j.ijheatfluidflow.2004.07.003.

Berana, M.S., Nakagawa, M., and Harada, A., 2009, "Shock waves in supersonic two-phase flow of CO2 in converging-diverging nozzles," *HVAC&R Research*, **15**(6), 1081–1098.
https://doi.org/10.1080/10789669.2009.10390880.

Brown, S., Martynov, S., Mahgerefteh, H., Chen, S., and Zhang, Y., 2014, "Modelling the non-equilibrium two-phase flow during depressurisation of CO2 pipelines," *International Journal of Greenhouse Gas Control*, **30**, 9–18.
https://doi.org/10.1016/j.ijggc.2014.08.013.

Croquer, S., Poncet, S., and Aidoun, Z., 2016a, "Turbulence modeling of a single-phase R134a supersonic ejector. Part 1: Numerical benchmark," *international journal of refrigeration*, **61**, 140–152.
https://doi.org/10.1016/j.ijrefrig.2015.07.030.

Croquer, S., Poncet, S., and Aidoun, Z., 2016b, "Turbulence modeling of a single-phase R134a supersonic ejector. Part 2: Local flow structure and exergy analysis," *international journal of refrigeration*, **61**, 153–165.
https://doi.org/10.1016/j.ijrefrig.2015.07.029.

Du, M., and Hu, J., 2020, "Effect of Residual Non-Condensable Gases on the Performance of a Carbon Dioxide Evaporator and the System Performance," *Frontiers in Heat and Mass Transfer (FHMT)*, **14**.
http://dx.doi.org/10.5098/hmt.14.5.

Gerber, A., 2008, "Inhomogeneous multifluid model for prediction of nonequilibrium phase transition and droplet dynamics," *Journal of Fluids Engineering*, **130**(3).
https://doi.org/10.1115/1.2844580.

Geuzaine, C., and Remacle, J.F., 2009, "Gmsh: A 3-D finite element mesh generator with built-in pre-and post-processing facilities," *International journal for numerical methods in engineering*, **79**(11), 1309–1331.
https://doi.org/10.1002/nme.2579.

Giacomelli, F., Mazzelli, F., Banasiak, K., Hafner, A., and Milazzo, A., 2019, "Experimental and computational analysis of a R744 flashing ejector," *International Journal of Refrigeration*, **107**, 326–343.
https://doi.org/10.1016/j.ijrefrig.2019.08.007.

Grübel, M., Starzmann, J., Schatz, M., and Vogt, D.M., 2018, "Modelling of condensing steam flows in Laval nozzles with ANSYS CFX," *Proceedings of the Institution of Mechanical Engineers, Part A: Journal of Power and Energy*, **232**(5), 571–575.
https://doi.org/10.1177/0957650917730664.

Haida, M., Smolka, J., Hafner, A., Palacz, M., Banasiak, K., and Nowak, A.J., 2018, "Modified homogeneous relaxation model for the R744 transcritical flow in a two-phase ejector," *International Journal of Refrigeration*, **85**, 314–333.
https://doi.org/10.1016/j.ijrefrig.2017.10.010.

Hill, P.G., 1966, "Condensation of water vapour during supersonic expansion in nozzles," *Journal of Fluid Mechanics*, **25**(3), 593–620.
https://doi.org/10.1017/s0022112066000284.

Jianxin, P., and Yigang, L., 2009, "Estimation of the surface tension of liquid carbon dioxide," *Physics and Chemistry of Liquids*, **47**(3), 267–273.
https://doi.org/10.1080/00319100701824389.

Lemmon, E., Bell, I.H., Huber, M., and McLinden, M., 2018, "NIST Standard Reference Database 23: Reference Fluid Thermodynamic and Transport Properties-REFPROP, Version 10.0, National Institute of Standards and Technology," *Standard Reference Data Program, Gaithersburg*.
http://dx.doi.org/10.18434/T4JS3C.

Lettieri, C., Yang, D., and Spakovszky, Z., 2015, "An investigation of condensation effects in supercritical carbon dioxide compressors," *Journal of Engineering for Gas Turbines and Power*, **137**(8), 082602.
https://doi.org/10.1115/1.4029577.

Lettieri, C., Paxson, D., Spakovszky, Z., and Bryanston-Cross, P., 2018, "Characterization of nonequilibrium condensation of supercritical carbon dioxide in a de laval nozzle," *Journal of Engineering for Gas Turbines and Power*, **140**(4), 041701.
https://doi.org/10.1115/1.4038082.

Mazzelli, F., Giacomelli, F., and Milazzo, A., 2018, "CFD modeling of condensing steam ejectors: Comparison with an experimental test-case," *International Journal of Thermal Sciences*, **127**, 7–18.
https://doi.org/10.1016/j.ijthermalsci.2018.01.012.

Mazzelli, F., Little, A.B., Garimella, S., and Bartosiewicz, Y., 2015, "Computational and experimental analysis of supersonic air ejector: Turbulence modeling and assessment of 3D effects," *International Journal of Heat and Fluid Flow*, **56**, 305–316.
https://doi.org/10.1016/j.ijheatfluidflow.2015.08.003.

Miqueu, C., Broseta, D., Satherley, J., Mendiboure, B., Lachaise, J., and Graciaa, A., 2000, "An extended scaled equation for the temperature dependence of the surface tension of pure compounds inferred from an analysis of experimental data," *Fluid phase equilibria*, **172**(2), 169–182. https://doi.org/10.1016/s0378-3812(00)00384-8.

Moses, C., and Stein, G., 1978, "On the growth of steam droplets formed in a Laval nozzle using both static pressure and light scattering measurements," *Journal of Fluids Engineering*, **100**(3), 311–322. https://doi.org/10.1115/1.3448672.

Nakagawa, M., Serrano, M.S., and Harada, A., 2008, "Shock waves in supersonic two-phase flow of CO2 in converging-diverging nozzles," *International Refrigeration and Air Conditioning Conference*, 2362, Purdue University e-Pubs.

Nouri-Borujerdi, A., and Ghazani, A.S., 2017, "Equilibrium and non-equilibrium gas–liquid two phase flow in long and short pipelines following a rupture," *AIChE Journal*, **63**(7), 3214–3223. https://doi.org/10.1002/aic.15675.

Palacz, M., Haida, M., Smolka, J., Nowak, A.J., Banasiak, K., and Hafner, A., 2017, "HEM and HRM accuracy comparison for the simulation of CO2 expansion in two-phase ejectors for supermarket refrigeration systems," *Applied Thermal Engineering*, **115**, 160–169. https://doi.org/10.1016/j.applthermaleng.2016.12.122.

Palacz, M., Smolka, J., Fic, A., Bulinski, Z., Nowak, A.J., Banasiak, K., and Hafner, A., 2015, "Application range of the HEM approach for CO2 expansion inside two-phase ejectors for supermarket refrigeration systems," *International Journal of Refrigeration*, **59**, 251–258. https://doi.org/10.1016/j.ijrefrig.2015.07.006.

Pang, A.L.J., Skote, M., and Lim, S.Y., 2016, "Modelling high Re flow around a 2D cylindrical bluff body using the k-ω (SST) turbulence model," *Progress in Computational Fluid Dynamics, an International Journal*, **16**(1), 48–57. https://doi.org/10.1504/pcfd.2016.074225.

Smolka, J., Bulinski, Z., Fic, A., Nowak, A.J., Banasiak, K., and Hafner, A., 2013, "A computational model of a transcritical R744 ejector based on a homogeneous real fluid approach," *Applied Mathematical Modelling*, **37**(3), 1208–1224. https://doi.org/10.1016/j.apm.2012.03.044.

Soave, G., 1972, "Equilibrium constants from a modified Redlich-Kwong equation of state," *Chemical engineering science*, **27**(6), 1197–1203. https://doi.org/10.1016/0009-2509(72)80096-4.

Starzmann, J., Hughes, F.R., Schuster, S., White, A.J., Halama, J., Hric, V., Kolovratník, M., Lee, H., Sova, L., ŠtâĂŹastnỳ, M., *et al.*, 2018, "Results of the international wet steam modeling project," *Proceedings of the Institution of Mechanical Engineers, Part A: Journal of Power and Energy*, **232**(5), 550–570. https://doi.org/10.1177/0957650918758779.

Wen, C., Karvounis, N., Walther, J.H., Yan, Y., Feng, Y., and Yang, Y., 2019, "An efficient approach to separate CO2 using supersonic flows for carbon capture and storage," *Applied energy*, **238**, 311–319. https://doi.org/10.1016/j.apenergy.2019.01.062.

Xiao, R., Jin, W., Han, S., Li, R., and Cao, X., 2017, "Numerical simulation on condensing flow of water vapor of wet natural gas inside the nozzle," *Frontiers in Heat and Mass Transfer (FHMT)*, **9**(1). http://dx.doi.org/10.5098/hmt.9.6.

Zheng, H., Ma, Y., Mei, H., Xu, X., Chen, X., and Cao, X., 2018, "Supersonic Condensation Characteristics of CO2 in Natural Gas Under Different Temperature Conditions," *Frontiers in Heat and Mass Transfer (FHMT)*, **11**. http://dx.doi.org/10.5098/hmt.11.34.